Title	Comparative analysis of the cellular entry of polystyrene and gold nanoparticles using the freeze concentration method
Author(s)	Ahmed, Sana; Okuma, Koyo; Matsumura, Kazuaki
Citation	Biomaterials Science, 6: 1791-1799
Issue Date	2018-04-30
Type	Journal Article
Text version	author
URL	http://hdl.handle.net/10119/15878
Rights	Copyright (C) 2018 Royal Society of Chemistry. Sana Ahmed, Koyo Okuma and Kazuaki Matsumura, Biomaterials Science, 6, 2018, 1791-1799. http://dx.doi.org/10.1039/C8BM00206A - Reproduced by permission of The Royal Society of Chemistry
Description	

1 **Comparative analysis of the cellular entry of polystyrene and gold nanoparticles**

2 **using the freeze concentration method**

3 *Sana Ahmed, Koyo Okuma, and Kazuaki Matsumura**

4

5 School of Materials Science, Japan Advanced Institute of Science and Technology, Nomi,

6 Ishikawa 923-1292, Japan

7

10 **E mail**: mkazuaki@jaist.ac.jp

11

12

13

14

15

16

17

18

19

20

21

22

23

1 **Abstract**

2 Despite advances in nanoparticle delivery, established physical approaches, such as

3 electroporation and sonication, result in cell damage, limiting their practical applications.

4 In this study, we proposed a unique freeze concentration-based technique and evaluated

5 the efficacy of the method using two types of nanoparticles, citrate-capped gold

6 nanoparticles and carboxylated polystyrene nanoparticles. We further compared the

7 internalisation behaviour of particles of various sizes with and without freezing. Confocal

8 microscopic images showed that the uptake efficacy for nanomaterials of 50 nm was

9 greater than that of l00-nm particles. Polystyrene nanoparticles of 50 nm had more

10 favourable adsorption and internalisation behaviours compared to those of gold

11 nanoparticles after freeze concentration. We also examined the possible endocytic

12 pathways involved in the uptake of gold and polystyrene nanoparticles, and found that

13 the route differed between unfrozen and frozen conditions. Overall, we determined the

14 influence of the freeze concentration strategy on both nanomaterial internalisation and

15 the endocytic uptake pathway. Our findings provide a mechanistic understanding of the

16 internalisation of nanoparticles using a freezing approach and thereby contribute to

17 further developments in nanotherapeutic applications.

18

19

20

21

22

23

24

25

26

27

Introduction

Recently, functional nanomaterials have gained substantial interest as diagnostic tools and for the development of delivery systems.[1] Among nanoparticles, gold[2] (Au) and polystyrene[3] (PS) nanoparticles are common nanocarriers for the delivery of a variety of biomacromolecules inside cells. Au nanoparticles are beneficial for various applications, such as biosensors,[4] antimicrobial agents,[5] tumour imaging,[6] and drug delivery.[7] PS with fluorescence plays an important role in dynamic interactions between nano-bio interfaces, has good biocompatibility and high stability, and is useful for cell imaging.[8]

However, nanomaterials have to cross the cell membrane to enter cells. To achieve this, physical approaches, such as electroporation[9] and sonication,[10] have been used for the delivery of nanomaterials of different sizes. A few studies have indicated that the use of electric fields might damage cells.[11,12] Therefore, we have developed a new freeze concentration-based strategy for the safe and effective delivery of proteins.[13-16] Freeze concentration is a physical process in which extremely low temperatures result in the transformation of water into ice crystals and the ejection of the protein-nanocarrier complex, thereby increasing the concentration of the protein-nanocarrier complex at the peripheral cell membrane. We previously demonstrated the benefits of the enhanced concentration of the protein-nanocarrier in immunotherapy[15] as well as in gene delivery systems.[16] However, the influence of the size and concentration of particles induced by freezing on the endocytic pathway has not been evaluated, and comparisons between non-frozen and frozen conditions are needed.

Endocytosis is a well-characterised pathway by which particles efficiently enter living cells. Plasma membranes are selectively permeable. Materials are usually enclosed by a small portion of the plasma membrane, initially invaginated, and then pinched off to form an endocytic vesicle that includes the ingested substance. [17,18] Nearly all types of cells utilise the endocytic pathway to communicate with viruses and nanoparticles.[19] Particles can be internalised into cells via two major pathways, i.e. phagocytosis and pinocytosis.[20] Large particles with a diameter of greater than 200 nm are usually taken up by phagocytosis. Some internalised vesicles never reach lysosomes because they are recovered by phagosomes vesicles and returned to the plasma membrane.[21] The majority of small particles enter via pinocytosis pathways, including macropinocytosis, clathrin-

mediated endocytosis, and caveolae-mediated endocytosis.[22] Typically, for clathrin mediated endocytosis, the endocytic cycle starts at clathrin-coated pits in small areas of the plasma membrane. Caveolae are present in the plasma membrane of all cell types. They are formed from lipid rafts (patches of plasma membrane) containing cholesterol, glycosphingolipids, and GPI-anchored membrane proteins. Macropinocytosis begins with the deformation of the plasma membrane; linear or curved ruffles form on cell membrane, and these constrict and become separated from the plasma membrane to form macropinosomes inside of cells.[23,24]

In general, physical approaches, e.g. electroporation and sonication, promote nanomaterial uptake via non-endocytic pathways, resulting in high oxidative stress and changes in cell stimuli.[25,26] The enhanced concentration of materials in the peripheral membrane using the freezing strategy enables uptake by endocytic pathways, as demonstrated in our previous research.[14] However, the precise effects of particle size and frozen or non-frozen conditions are unclear. Therefore, to elucidate the effect of particle concentration using freezing and non-freezing systems and the influence of size, we used citrate-capped Au nanoparticles and carboxylated PS nanoparticles as model systems.

In this study, we evaluated two types of particles, i.e. inorganic nanoparticles and polymeric nanoparticles. A number of inorganic particles, such as silver nanoparticles (Ag), are used in biomedical applications owing to their beneficial properties, including their antibacterial effects.[27] For example, the nanohybrid Ag@PS complex with a nitroxide linker provides efficient activity against pathogenic bacteria.[28] Many previous studies have assessed the influence of various factors associated with the cellular uptake of fluorescent latex particles (PS beads).[29,30] Haines et al. demonstrated the effects of particle size, cell line, and even cell density on the uptake of PS microspheres.[29] In another study, Florence et al. showed the size dependency of microspheres on uptake in systematic organs after oral administration; particles exceeding 100 nm did not reach the bone marrow and those exceeding 300 nm were absent from blood.[30]

In our study, we focused on Au nanoparticles and PS nanoparticles owing to their availability in a variety of sizes and surface chemistries; we used the fibroblast L929 cell line and the freeze concentration approach to study the endocytic mechanism. To the best of our knowledge, this is the first study to demonstrate that the freeze concentration

approach induces different endocytic pathways depending on the material and size. For consistency, both types of nanomaterials (Au and PS nanoparticles) had similar hydrodynamic sizes, i.e. they were 50 and 100 nm in diameter, for investigation of uptake by fibroblast L929 cells using non-frozen and frozen approaches; furthermore, we discuss the potential endocytic mechanisms in these conditions.

Experimental

Reagents

Citrate buffer-stabilised gold nanoparticles (50 and 100 nm), filipin, and EIPA (5-(*N*-ethyl-*N*-isopropyl)-amiloride) were obtained from Sigma Aldrich (St. Louis, MO, USA). Fluoresbrite® Yellow Green Polybead Microspheres (YG Polybeads, λ_{ex} = 441 nm, λ_{em} = 486 nm) with diameters of 50 and 100 nm were purchased from Polyscience Inc. (Warrington, PA, USA). Chlorpromazine and DMSO were obtained from Nacalai Tesque (Kyoto, Japan).

Zeta potential and hydrodynamic size of gold and polystyrene nanoparticles

The average hydrodynamic diameter and zeta potential of Au and PS nanoparticles were measured by dynamic light scattering (DLS) using the Zetasizer 3000 (Malvern Instruments, Worcestershire, UK) with a scattering angle of 135°. Results were obtained as the average of three measurements using different samples.

Transmission electron microscopy (TEM)

Au and PS nanoparticle solutions (10 μL) were placed on a copper grid (NS-C15 Cu150P; Stem, Tokyo, Japan). In the case of PS nanoparticles, the grids were negatively stained with 2% phosphotungstic acid (Sigma Aldrich, Steinheim, Germany) for 1 min and then washed with two drops of distilled water, blotted, and air-dried. TEM images were obtained using a Hitachi H-7100 system (Tokyo, Japan) with an accelerating voltage of 100 kV.

Cell culture

L929 cells (American Type Culture Collection, Manassas, VA, USA) were cultured in Dulbecco's modified Eagle's medium (DMEM; Sigma-Aldrich) supplemented with 10% foetal bovine serum (FBS) at 37°C and 5% CO_2 in a humidified atmosphere. When the cells reached 80% confluence, they were removed using 0.25% (w/v) trypsin containing 0.02% (w/v) ethylenediamine tetraacetic acid (EDTA) in phosphate-buffered saline without calcium and magnesium (PBS(-)) and were seeded on a new tissue culture plate for subculture.

Cellular adsorption of nanoparticles by freeze concentration

L929 cells were counted and re-suspended in 1 mL of 10% DMSO (without FBS) containing Au or PS (2–10×10^{10} particles/mL) nanoparticles at a density of 1×10^6 cells/mL in 1.9-mL cryovials (Nalgene, Rochester, NY, USA) and were stored in a -80°C freezer overnight. The vials were thawed at 37°C, diluted with DMEM, and cells were washed 3 times with DMEM containing 10% FBS. Subsequently, cells were counted using a haemocytometer by the trypan blue staining method. Cell viability was determined as the ratio of living cells to total cells. The adsorption of nanoparticles on L929 cells before and after freezing was observed using a confocal laser scanning microscope (CLSM) (FV1000-D; Olympus, Tokyo, Japan). The PS nanoparticles were internally labelled by Yellow Green, similar to FITC (fluorescein isothiocyanate) fluorophores, with (YG Polybeads, λ_{ex} = 441 nm, λ_{em} = 486 nm). Au nanoparticles were quantitatively evaluated by plasmon scattering. Au nanoparticles of 50 nm and 100 nm were irradiated using a laser wavelength of 559 nm.

Internalisation of nanoparticles by freeze concentration

After the thawing procedure, the cells were washed three times using cell culture medium with 10% FBS. Then, the cells were again seeded on a 35-mm glass-bottom dish with DMEM. After incubation for 24 h, the attached cells were washed with PBS (-) 3 times and were observed using a CLSM. For comparisons with non-frozen cells as a control, the same concentration of nanoparticles was added to the L929 cell suspension, centrifuged at $112 \times g$, washed with medium, and seeded them for 24 h. All cells were washed with PBS (-) before the observation of internalisation using a CLSM.

Elucidation of the internalisation pathway in non-frozen and frozen conditions by an inhibition assay

L929 fibroblast cells were pre-treated with various concentrations of endocytic inhibitors, including chlorpromazine (12.5 µM), EIPA (125 µM), and filipin (2.5 µM). Previously reported inhibitor concentrations were used.[14] Then, the samples were cryopreserved with 10% DMSO carrying Au or PS nanoparticles in the cell culture medium at −80°C. Solutions were thawed and the cells were counted to determine the toxicity of the inhibitors using the trypan blue exclusion assay. After the addition of particular inhibitors, cells at a density of 1×10^6 cells per mL were seeded on a glass-bottom dish for 24 h to investigate the uptake of particles. The same procedure was applied for the non-frozen condition. The nanoparticles with inhibitors were gently added to fibroblast cells and seeded on glass-bottom dishes following the same methods. Cells treated with only Au or PS nanoparticles were regarded as positive controls. After incubation, cells were washed with PBS (-) 3 times to remove any traces of inhibitors. The mean scattering of Au nanoparticles per cell was detected by excitation at 559 nm using a confocal microscope. A similar procedure was applied for PS nanoparticles; the quantification of the mean fluorescence intensity per cell was performed using a confocal microscope.

Statistical analysis

All data are expressed as means ± standard deviation (SD). All experiments were conducted in triplicate. For comparisons among groups, a one-way analysis of variance with a post-hoc Fisher's protected least significant difference test was used. Differences were considered statistically significant when $p < 0.05$.

Results and discussion

Hydrodynamic size and zeta potential of gold and polystyrene nanoparticles in the presence of cryoprotectants

We checked the actual sizes of Au and PS nanoparticles by TEM and the results are shown in **Figure S1**. Both Au and PS nanoparticles had uniform sizes of 50 nm and 100 nm. Our

main aim was to use the freeze concentration procedure for the internalisation of Au and PS nanoparticles of various sizes. However, the colloidal stability of these nanoparticles is a major challenge in frozen conditions.[31] At the time of freezing, the nanoparticle concentration increases due to solute exclusion from ice crystal formation. This stress could affect the ionic strength, size, and surface potential of nanoparticles.[32] A variety of cryoprotectants have been used to shield nanoparticles during freezing.[33] Therefore, we investigated the aggregation behaviour of Au and PS nanoparticles in response to freeze concentration and determined suitable conditions for minimising irreversible aggregation. We used DMSO, a well-established cryoprotectant for cell storage.[34] We evaluated the size and surface charge of particles in non-frozen and frozen conditions. Au and PS nanoparticles (2×10^{10} particles/mL) were dispersed in 1 mL of milli-Q water and the hydrodynamic sizes and zeta potential were determined by the DLS technique. As shown in **Figure S2A**, the hydrodynamic sizes of Au nanoparticles (2×10^{10} particles/mL) were around 60 nm and 130 nm, consistent with the expectation at room temperature in the absence of a cryoprotectant for 50- and 100-nm Au nanoparticles. When Au nanoparticles were frozen in the presence of 10% DMSO, their sizes did not change substantially. We also evaluated the influence of freezing on the surface charge of 50- and 100-nm Au nanoparticles. As expected, the zeta potential was negative due to the efficient distribution of citrate groups in Au nanoparticles, even during freezing. The zeta potential was -24.3 ± 8.0 mV for 50-nm Au nanoparticles at room temperature, but was -16.4 ± 4.6 mV for 100-nm Au nanoparticles. When nanoparticles were frozen at -80°C in the presence of 10% DMSO as a cryoprotectant, the surface potential was nearly equal to that in normal conditions. These results suggested that freezing and cryoprotectants do not have a substantial influence on zeta potential, and particles retain their anionic property (**Figure S2 b**).

We also characterised the hydrodynamic size and zeta potential of PS nanoparticles (**Figure S2C and D**). With respect to the size of PS nanoparticles in aqueous medium, the results were similar to those obtained for Au nanoparticles. At room temperature, the hydrodynamic size of polystyrene nanoparticles was approximately 71.6 ± 1.1 nm in the case of 50-nm nanoparticles. The hydrodynamic size of approximately 152.4 ± 16.7 nm was slightly greater than the actual size of 100 nm of polystyrene nanoparticles (**Figure S2C**). We also evaluated the influence of freezing on the surface potential of PS

nanoparticles and found that the potential was nearly the same in the presence of 10% DMSO and at room temperature (**Figure S2 D).**

Since the estimates of size and potential were similar and consistent with the TEM results, it is difficult to determine whether the cryoprotectant contributes to aggregation (**Figure S2A–D**). These results indicated that 10% DMSO is inert and does not affect colloidal stability for both Au and polystyrene nanoparticles.

Gold and polystyrene nanoparticle adsorption on L929 cells using the freeze concentration approach

Next, we investigated the efficacy of the freeze concentration method for the in vitro delivery of two different materials. We chose L929 fibroblasts as a model cell line to evaluate the effects of different materials with different sizes in a single cell line. L929 cell line can be easily cultured in a reproducible manner. Also, this cell lines are widely used for preliminary studies for wide range of biomaterials due to easily proliferation and adherence on the biomaterials surface. In our previous studies, we also chose L929 cell line for our research.[13,14] To evaluate cell viability, L929 cells were mixed with various concentrations of 50-nm and 100-nm Au and PS nanoparticles that were cryopreserved with 10% DMSO in culture medium without FBS. Cell viability was then calculated using trypan blue staining solution after thawing. As shown in **Figure S3,** cell viability decreased as the concentration of nanoparticles (Au and PS) increased (**Figure S3A–B**). A low concentration of nanoparticles for both sizes resulted in a cell viability of around 80%. We used small concentrations of Au and PS nanoparticles for in vitro delivery.

Interestingly, we observed that cell viability was lower for small nanoparticles than for large nanoparticles. This result is in agreement with previous studies indicating that smaller nanoparticles are generally more toxic.[35] Likewise, as shown in **Figure S3 B**, cell viability for 100-nm PS beads was significantly greater than that for 50-nm PS beads at every concentration, suggesting that cytotoxicity in greater for the latter than the former. This result was consistent with the findings of Jeong et al., who found that microbead toxicity is size-dependent and smaller microbeads are more toxic.[36] It is worth pointing out that although our nanoparticles had negative charges of different values, size was the predominant determinant of cytotoxicity.

We then used the freeze concentration methodology to investigate adsorption behaviour on cell membranes. A brief illustration of the protocol is shown in **Scheme 1**. First, we determined the effect of freezing on the adsorption efficacy of Au nanoparticles. The Au nanoparticles did not require modification with fluorescent dyes owing to their intrinsic optical properties (plasmon scattering). Scattering images can be easily observed for Au nanoparticles at a laser wavelength of 559 nm for excitation. Many studies have evaluated nanoparticles inside cells by utilising plasmon scattering properties.[37] Scattered Au nanoparticles of both sizes (50 and 100 nm) were efficiently visualised by confocal microscopy after freeze concentration, as shown in **Figure 1**. The non-frozen conditions did not influence the absorption of Au nanoparticles around the cell membrane for both 50 and 100 nm (**Figure 1A and C**). However, Au internalisation increased when using the freezing approach (**Figure 1B and C**).

We also quantified the mean scattering intensity of Au nanoparticles for Au nanoparticles of 50 and 100 nm by confocal microscopy. We found greater intensities for frozen Au nanoparticles than non-frozen nanoparticles, indicating increased adsorption on the cell surface (**Figure 1E**).

Furthermore, the adsorption of PS nanoparticles of both 50 and 100 nm was greater in frozen than in non-frozen conditions (**Figure 2A–D**). Quantification by confocal microscopy revealed that the freezing technique increases the penetration of PS nanoparticles **(Figure 2E).**

When cells and nanoparticles are subjected to an ultra-cold environment, water in the system is converted into ice crystals, leading to an increased concentration of nanoparticles in the extracellular solution. The increased concentration of nanoparticles leads to increased interactions with the cell membrane in the frozen system, thereby promoting the efficient adsorption of particles. Although negatively charged nanoparticles are expected to be less efficiently adsorbed by a negatively charged cell membrane, the cellular adsorption of negatively charged NPs was high, possibly due to strong, localised, and nonspecific interactions with the plasma membrane.[38] Taken together, these results indicate that the freeze-concentration method enhances the association of both Au and PS nanoparticles on cells, while maintaining a high cell viability.

Intracellular delivery of gold and polystyrene nanoparticles using L929 cells by freeze concentration

The adsorption of nanoparticles on the cell membrane was enhanced using the freeze concentration approach. Usually, the internalisation of nanoparticles in cells is very important for achieving a therapeutic effect. To investigate this, a similar protocol was applied to that summarised in **Scheme 1.** The confocal microscopic images for the internalisation of Au and PS nanoparticles are shown in **Figure 3A–H**. The results were quite similar to those shown in **Figure 1 and 2.** Both Au and PS nanoparticles were efficiently internalised into cells (**Figure 3B, D, F, H**). However, the non-freezing approach did not induce internalisation for similar conditions (**Figure 3A, C, E, G).** Moreover, greater internalisation was observed for smaller Au and PS particles than for large particles. **Figure 3I** summarises the quantitative analysis of intensity values obtained by confocal microscopy for PS and Au nanoparticles at 50 and 100 nm. Interestingly, we found higher intensities using 50-nm PS nanoparticles than using other materials for both the non-frozen and frozen systems. Various studies have reported that small particles are efficiently taken up by cells, in general.[17,39,40]

Nanoparticle size is an important determinant of cellular internalisation. Chithrani et al. showed that 50-nm transferrin-coated Au nanoparticles exhibit greater uptake than that of 100 nm particles. They attributed this to the "wrapping effect," which induces more efficient cell internalisation. Additionally, they described the roles of ligand-receptor interactions as well as receptor diffusion kinetics in cellular internalisation. The so called "Wrapping effect" indicated how the cellular membrane encloses nanoparticles. Two Factors are associated with the term "Wrapping effect" wherein it dictates the free energy for ligand-receptor interaction and other is the receptor diffusion kinetics onto wrapping sites around the cellular membranes. [41]

It should be noted that PS nanoparticles have increased interactions with the plasma membrane compared with Au nanoparticles. The increased internalisation of PS nanoparticles might be explained by the difference in affinity towards the cell membrane.

Endocytosis mechanisms

A better understanding of the interactions of functional nanoparticles with biological cells is needed not only for the development of new methods for imaging and therapy, but also to improve our knowledge of the fundamental cellular mechanisms and cytotoxicity of nanomaterials. Therefore, we evaluated the effects of the freeze concentration method on endocytic pathways. Various endocytic inhibitors, such as chlorpromazine (for clathrin-mediated endocytosis), EIPA (for macropinocytosis), and filipin (for caveolae mediated endocytosis), were added to elucidate the endocytic pathway. Before evaluating the endocytic pathways, it is crucial to investigate the effects of these nanoparticles and inhibitors on cell viability, as these inhibitors are cytotoxic at particular concentrations. Hence, we evaluated cell viability using trypan-blue exclusion assays after freezing. The optimal concentration of inhibitors with respect to cell viability (**Figure 4**) was used to elucidate the endocytic pathway. Before freezing, the cells are 100% alive whereas after freezing the cells viability are slightly decrease even after adding cryoprotectant. We examined the endocytic mechanism for two different materials of different sizes and frozen as well as non-frozen conditions by fluorescent confocal microscopy. Quantitative results were obtained from confocal images, which are shown in the supporting information (**Figure S4A–D**). For both nanoparticle types, intensity was quantified by confocal microscopy (**Figure 5A–D)**. **Figure 5A and B** show the scattering intensity of Au nanoparticles in the presence of inhibitors for frozen and non-frozen conditions. A high scattering intensity was observed for L929 cells used as a positive control, without inhibitors. When particular inhibitors were added, a change in the scattering intensity was observed. A decreased intensity of Au nanoparticles in the presence of inhibitors implies that the particular inhibitor affected the uptake and restricted the entry of nanoparticles into the cell membrane. We observed a lower scattering intensity for 50 and 100 nm Au nanoparticles in the presence of chlorpromazine; this outcome suggested that chlorpromazine inhibits endocytosis. Accordingly, Au particles of 50 and 100 nm primarily enter cells via clathrin-mediated endocytosis (**Figure 5A**). Interestingly, using the freeze concentration approach, the 50-nm Au nanoparticles exhibited a decreased scattering intensity when the filipin inhibitor was applied, indicating that freezing induces a change in the uptake pathway to caveolae-mediated endocytosis (**Figure 5B**). Au nanoparticles of 100 nm showed a similar trend with respect to the alteration of pathways. For 100-nm particles, in non-frozen conditions,

clathrin-type endocytosis was dominant (**Figure 5A**). However, frozen conditions resulted in a shift to the caveolae as well as macropinocytosis pathways, even for 100-nm particles (**Figure 5B**).

The endocytic mechanism for PS-based nanomaterials differed somewhat from that for Au nanoparticles. The 50-nm PS nanoparticles tended to exhibit uptake by macropinocytosis pathways, as evidenced by the decreased fluorescence intensity in the presence of the EIPA inhibitor **(Figure 5C).** When the freezing approach was applied, the pathway changed to clathrin-mediated endocytosis (**Figure 5D**). PS nanoparticles of 100 nm were associated with both clathrin- and caveolae-dependent endocytosis in normal conditions **(Figure 5C).** In particular, the freeze concentration-mediated internalisation of PS nanoparticles occurred only by clathrin-mediated endocytosis (**Figure 5D**).

Previous reports have suggested that endocytic mechanisms are usually dependent on size and cell type.[42] However, these are not the only factors responsible for specific uptake. In one study, Mironava et al. reported that 45-nm Au NPs penetrated cells via clathrin-mediated endocytosis,[43] consistent with the results of our study. However, the frozen system changes the pathway for 50-nm Au nanoparticles. An increase in cell stress caused by the freeze process could explain the change in the endocytic pathway. Understanding the detailed determinants of the endocytic mechanism can clarify the importance of freeze concentration-induced changes in the endocytic pathway. The same trend was observed for particles of other sizes.

An "electroporation" method has previously been used to promote nanoparticle uptake into cells by applying external electrical impulses, resulting in transient membrane pores through which nanoparticles can easily pass.[44] Another approach, "microinjection", is a valuable tool to deliver molecules inside cells. These previous methods adopt a non-endocytic pathway that can induce significant tension, thereby disrupting the lipid bilayers and nanoscale hole formation around the cell membrane.[44, 45] These strategies result in substantial cell loss, deformation of the cell membrane, and the non-specific entry of materials, and accordingly they are not practical for applications in biomedical engineering.

In our study, a new "freeze concentration" method was developed that does not involve the direct entry of materials inside cells, but rather promotes the interaction between the cell membrane and materials. Compared with previously described physical approaches, this freezing strategy has several benefits, including its high reliability, low cost, and simplicity, using an external force to induce cell membrane interactions without toxicity.

Regardless, further detailed investigations are needed to elucidate the underlying mechanism by which freezing induces nanoparticle uptake via different pathways. Studies of nanoparticle internalisation by cells can provide a basis for understanding their ultimate sub-cellular fate and localisation. A comprehensive knowledge of how particle size and freezing conditions affect the interactions between cells and appropriate combinations of nanomaterials using the freeze concentration approach is crucial for delivery applications. In future studies, we will apply the approach to various cell lines, such as HeLa cells, SK-Mel-28 melanoma cells, and RAW 264.7 macrophages, to evaluate the endocytic entry of different materials using the freeze concentration approach.

Conclusion

Our results demonstrated that the freeze concentration strategy enables the efficient internalisation of Au and PS nanoparticles into fibroblast cells. DLS and zeta potential measurements showed that the colloidal stability of these nanomaterials is retained in the presence of 10% DMSO (a cryoprotectant) after freezing. Further, 50-nm PS nanoparticles showed high intracellular uptake efficacy, while 50-nm Au nanoparticles showed the lowest efficacy. We also investigated the endocytic uptake mechanism using frozen and non-frozen systems with a model fibroblast cell line. Interestingly, Au nanoparticles of both 50 and 100 nm exhibited clathrin-dependent endocytosis in non-frozen conditions, but freezing resulting in a change to the caveolae-dependent and macropinocytosis pathways. Other PS nanoparticles utilised a different endocytosis pathway depending on size and frozen conditions. Our results emphasise the importance of the physical "freezing" approach for nanomaterials of various sizes to guide endocytic uptake for efficient delivery systems. We expect that the precise information about the endocytic uptake of nanoparticles will facilitate the design of materials with increased cellular uptake and the use of the freeze concentration approach for extensive biomedical applications.

Conflicts of interest

There are no conflicts of interest to declare.

Acknowledgements

References

1. M. K. Yu, J. Park and S. Jon, *Thernostics*, 2012, **2**, 3-44.
2. S.Huo, S. Jin, X. Ma, X. Xue, K. Yang, A. Kumar, P.C. Wang, J. Zhang, Z.Hu and X.J. Liang, ACS *Nano*, 2014, **8**(6), 5852-5862.
3. K. Saralidze, L.H. Koole and M.L.W. Knetsch, *Materials*, 2010, **3**, 3537-3564.
4. X. Zhang, Q. Guo and D. Cui, *Sensors* (Basel), 2009, **9**(2), 1033-1053.
5. Y. Zhou, S. Kundu, J.D. Cirillo and H. Liang, *J Nanobiotechnology*, 2012, **10**, 1-9.
6. Y. Xing, J. Zhao, P.S. Conti and K. Chen, *Thernostics*, 2014, **4**(3), 290-306.
7. F.Y. Kong, J.W. Zhang, R.F. Li, Z.X. Wang, W.J. Wang and W. Wang, *Molecules*, 2017, **22**, 1-13.
8. K. Kenesei, K. Murali, A. Czeh, J. Piella, V. Puntes and E. Madarasz, *J Nanobiotechnology*, 2016, **14**, 1-14.
9. Y. Zu, S. Huang, W.C. Liao and S. Wang, *J Biomed Nanotechnol*, 2014, **10**(6), 982-992.
10. I. Lentacker, S.C. DeSmedt and N.N. Sanders, *Soft matter*, 2009, **5**, 2161-2170.
11. S. J. Beebe, N.M. Sain and W. Ren, *Cells*, 2013, **2**(1), 136-162.
12. W.S. Meaking, J. Edgerton, C.W. Wharton and R.A. Meldrum, *Biochim. Biophys. Acta*, 1995, **1264**, 357-362.
13. S. Ahmed, F. Hayashi, T. Nagashima and K. Matsumura, *Biomaterials*, 2014, **35**, 6508-6518.
14. S. Ahmed, S. Fujita and K. Matsumura, *Nanoscale*, 2016, **8**, 15888-15901.
15. S. Ahmed, S. Fujita and K. Matsumura, *Adv. Healthc. Mater.*, 2017, **6**, 1700207.
16. S. Ahmed, N.K. Tadashi, T. Watanabe, T. Hohsaka and K. Matsumura, *ACS Biomater. Sci. Eng.*, 2017, **3**(8), 1677-1689.

17. N. Oh and J.H. Park, *Int. J Nanomedicine* 2014, **9**, 51-63.

18. G. Sahay, D.Y. Alakhova and A.V. Kabanov, *J Control Release*, 2010, **145**(3), 182-195.

19. S.Xu, B.Z. Olenyuk, C.T. Okamoto and S.F. Hamm- Alvarez, *Adv. Drug Deliv. Rev.,* 2013, **65**(1), 121-138.

20. S. Kumari, S. MG and S. Mayor, *Cell Res.*, 2010, **20**, 256-275.

21. M.O. Oyewumi, A. Kumar and Z. Cui, *Expert Rev Vac.,* 2010, **9**(9), 1095-1107.

22. A. El-sayed and H. Harashima, *Mol Ther.*, 2013, **21**(6), 1118-1130.

23. B. Alberts, A. Johnson and J. Lewis, *Molecular Biology of the Cell.* 4th edition. Garland Science, New York, 2002.

24. T.P Welliver, S. L. Chang, J. L. Linderman and J.A. Swanson, *J Cell Sci.* 2011, **124**(23), 4106-4114.

25. X. Zhao, Y. Wu, D. Gallego-Perez, K.J. Kwak, C. Gupta, X. Quyang and L.J. Lee, *Anal Chem.*, 2015, **87**(6), 3208-3215.

26. P.E. Boukany, Y. Wu, X. Zhao, K.J. Kwak, P.J. Glazer, K. Leong and L.J. Lee, *Adv. Healthc Mater.*, 2013, **3**, 682-689.

27. P. Krystosiak, W. Tomaszewski and E. Megiel*, J Colloid Interface Sci.* 2017, **498**, 9-21.

28. M. Gozdziewska, G. Cichowicz, K. Markowska, K. Zawada and E. Megiel, *RSc Adv.* 2015, **5**, 58403-58415.

29. W. Zauner, N.A. Farrow and A.M. Haines, *J Control Release* 2001, **71**(1), 39-51.

30. P.Jani, G.W. Halbert, J. Langridge and A.T. Florence*, J Pharm Pharmacol.* 1990, **42**, 821-826.

31. M.J. Choi, S. Briancon, J. Andrieu, S.G. Min and H. Fessi, *Drying Technol.*, 2004, **22**, 335-346.

32. C. Vauthier, B. Cabane and D. Lanbarre, *Eur J Pharm Biopharm,* 2008, **69**(2), 466-475.

33. A.M. Alkilany, S.R. Abulateefeh, K.K. Mills, A.I.B. Yaseen, M.A. Hamaly, H.S. Alkhatib, K.M. Aiedeh and J.W. Stone, *Langmuir*, 2014, **30**, 13799-13808.

34. G. Chen, A. Yue, Z. Ruan, Y. Yin, R. Wang, Y. Ren and L. Zhu, *Stem cells Int.*, 2016, **7**, 1-7.

35. L. Yildirimer, N.T.K. Thanh, M. Oizidou and A.M. Seifalian, *Nano today*, 2011, **6**, 585-607.

36. C.B. Jeong, E.J. Won, H.M. Kang, M.C. Lee, D. Hwang and U.K. Hwang, *Environ Sci Technol.*, 2016, **50**(16), 8849-8857

37. M. Takahashi, P. Mohan, K. Mukai, Y. Takada, T. Matsumoto, K. Matsumura, M. Takakura, H. Arai, T. Taguchi and S. Maenosono, *ACS Omega*, 2017, **2**, 4929- 4937.

38. C. Billotey, C. Wilhelm, M. Devaud, J.C. Bacri, J. Bittoun and F. Gazeau, *Magn. Reson. Med.*, 2003, **49**, 646-654.

39. S. Zhang, J. Li, G. Lykotrafitis, G. Bao and S. Suresh, *Adv Mater.*, 2009 , **21**,419–424

40. L. Shang, K. Nienhaus and G.U. Nienhaus, *J. Nanobiotechnology*, 2014, **12**, 1-48.

41. B.D. Chithrani and W.C. Chan, *Nano Lett.* 2007, **7**(6), 1542-1550.

42. J. Giudice, E.A. Jares-Erijman and F.C. Leskow, *Bioconjugate Chem*, 2013, **24**(3), 431-442.

43. T. Mironava, M. Hadjiargyrou, M. Simon, V. Jurukovski and M.H. Rafailovich, *Nanotoxicology*, 2010, **4**,120–137.

44. C.P Jen, Y.H. Chen, C.S. Fan, C.S. Yeh, Y.C. Lin, D.B. Shieh, C.L. Wu, D.H. Chen and C.H. Chou, *Langmuir* 2004, **20**, 1369-1374.

45. G. Liu, D. Li, M. K. Pasumarthy, T. H. Kowalczyk, C. R. Gedeon, S. L. Hyatt, J. M. Payne, T. J. Miller, P. Brunovskis and T. L. Fink, *J Biol Chem.* 2003, **278**, 32578–32586.

Figures

Scheme-1 Protocol representation of nanoparticles adsorption and internalisation into fibroblast L929 cells by freeze concentration approach

Au 50 nm

Au 100 nm

18

(E)

1
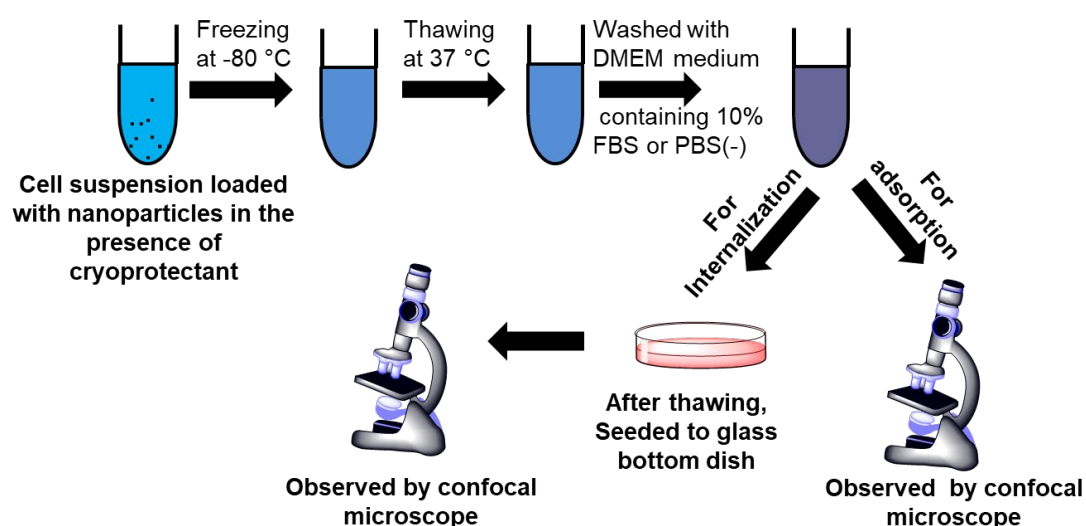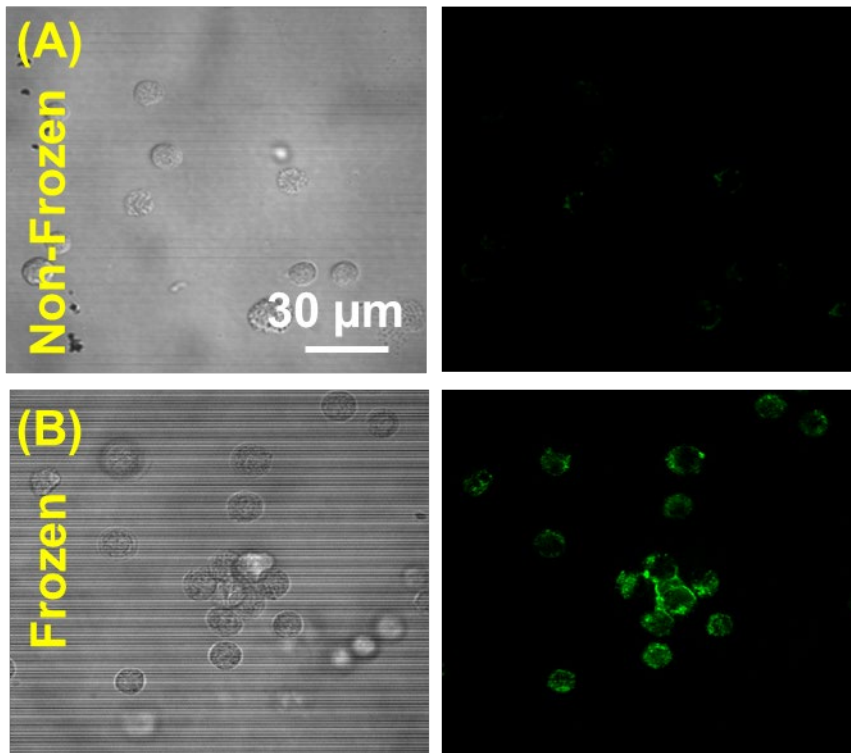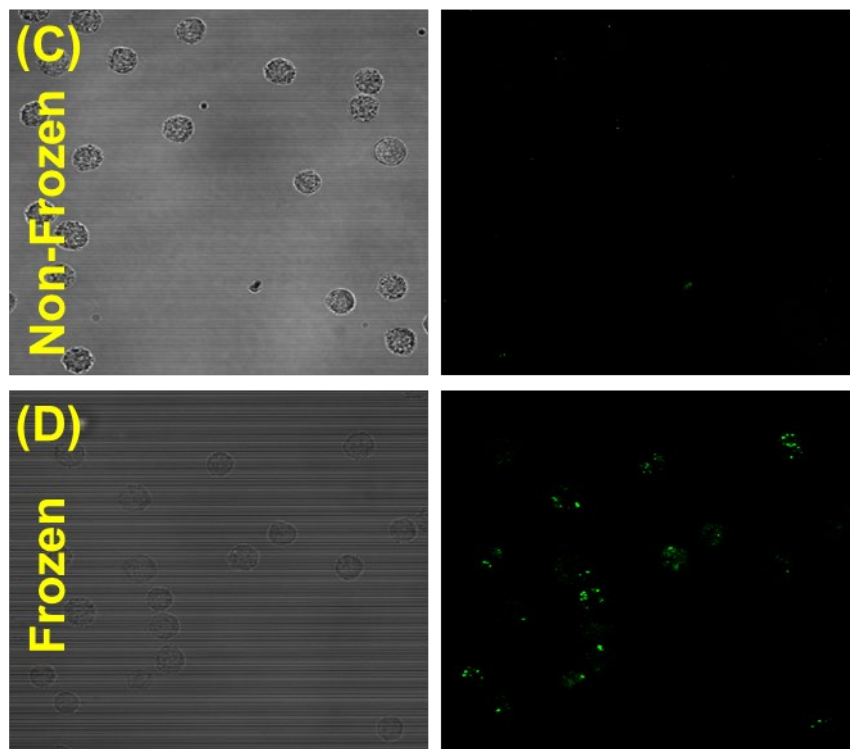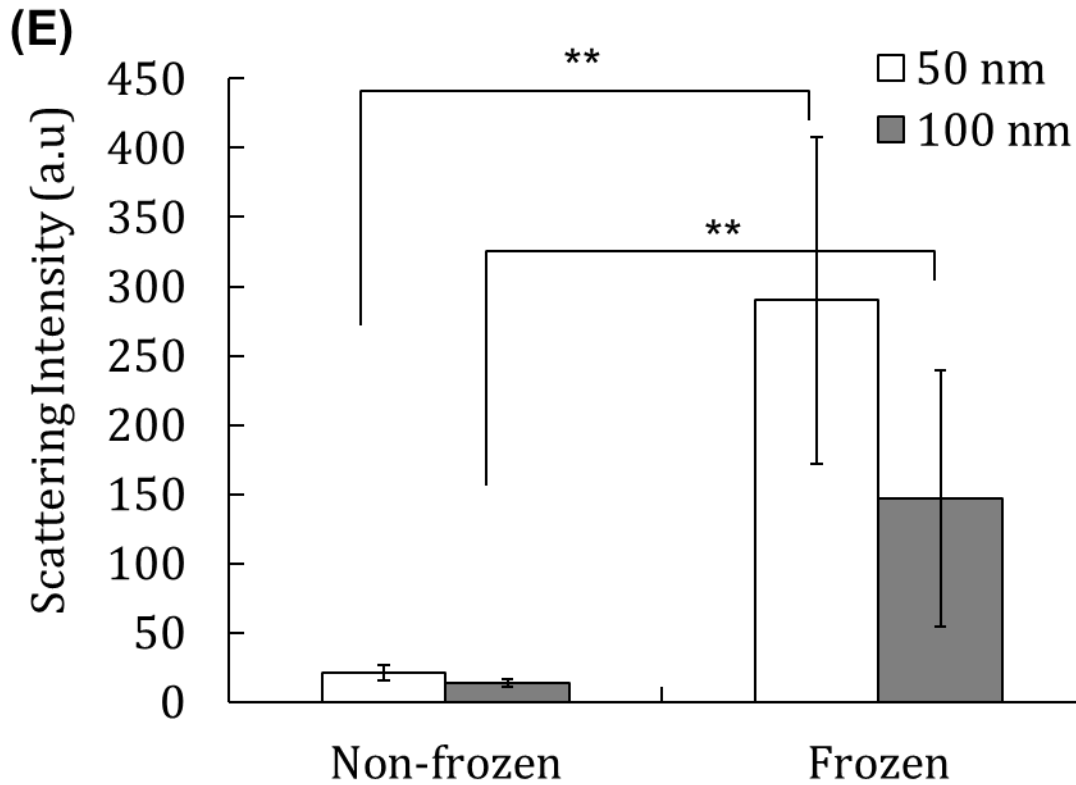
Figure 1 Confocal microscope images of Au nanoparticles of different sizes (50 and 100 nm) before and after freezing with 10% DMSO as a cryoprotectant to detect plasmon scattering from the Au nanoparticles of 50 nm and 100 nm. (A, B) Non-frozen and frozen 50 nm Au. (C, D) Non-frozen and frozen 100 nm Au. Scale bar: 30 μm (E) Mean scattering intensity of Au nanoparticles determined by confocal microscopy. Results are expressed as means ± SD. **$p < 0.01$

PS 50 nm

PS 100 nm

(E)
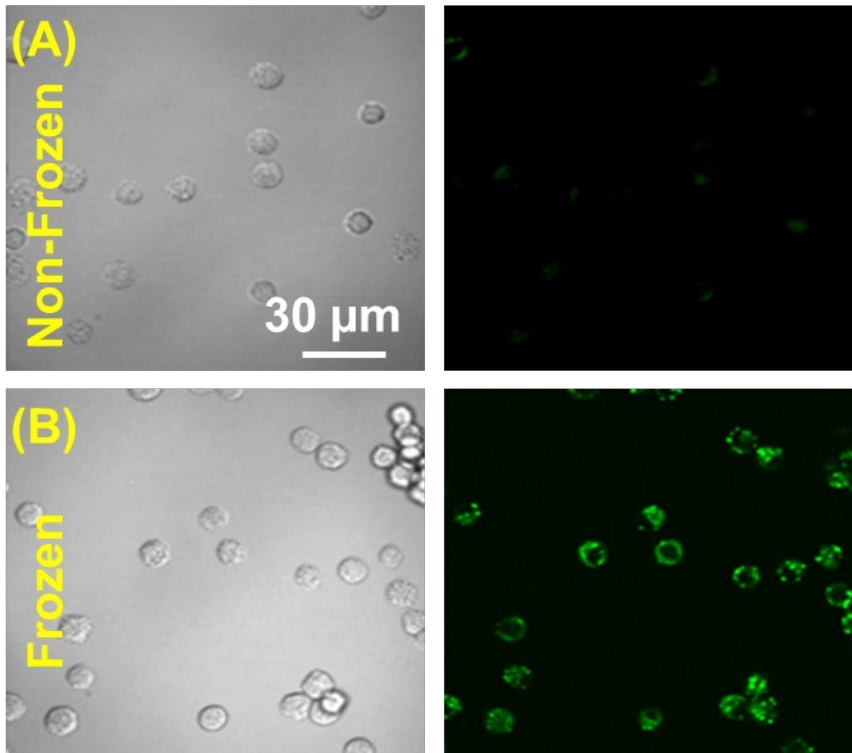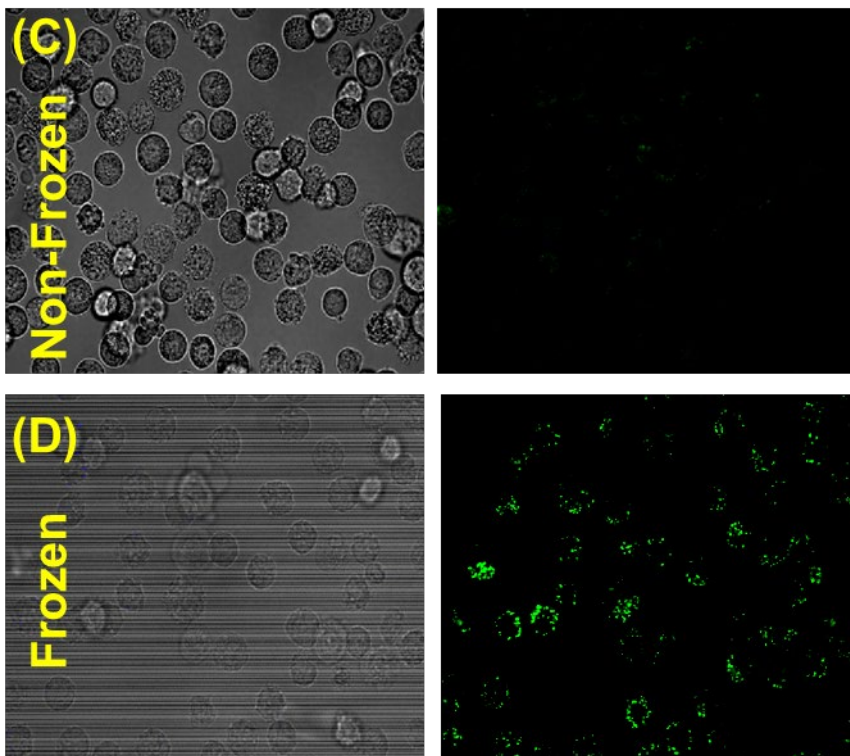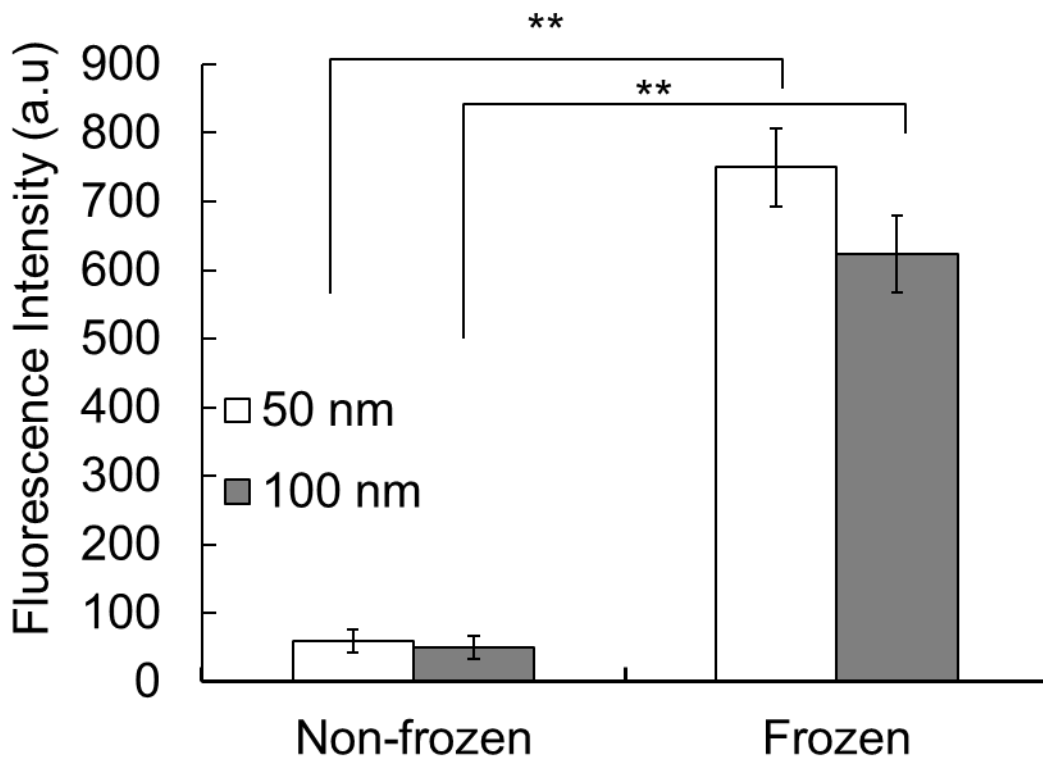
Figure 2 Confocal microscope images of PS nanoparticles of different sizes (50 and 100 nm) before and after freezing with 10% DMSO as a cryoprotectant. (A, B) Non-frozen and frozen 50-nm PS nanoparticles. (C, D) Non-frozen and frozen 100-nm PS nanoparticles. Scale bar: 30 μm (E) Mean fluorescence intensity of PS nanoparticles investigated by confocal microscopy. Results are expressed as means ± SD. **$p < 0.01$

Au nanoparticles 50 nm

Bright field	Au scattering

(A) Non-frozen

30 μm

(B) Frozen

1
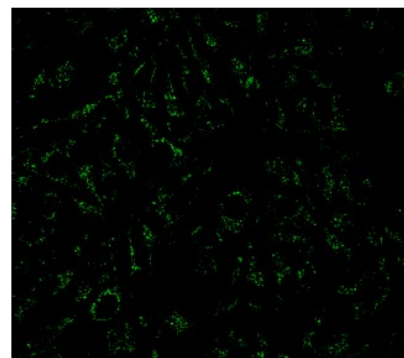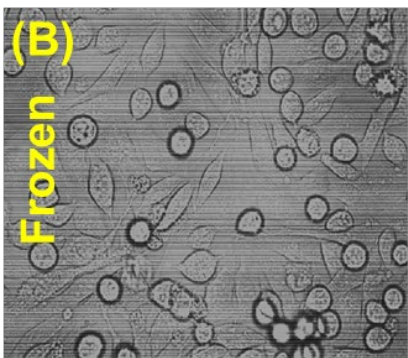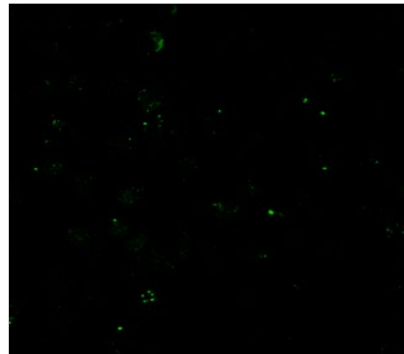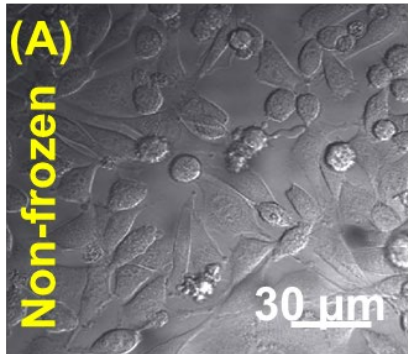
Au nanoparticles 100 nm

(C) Non-Frozen

(D) Frozen
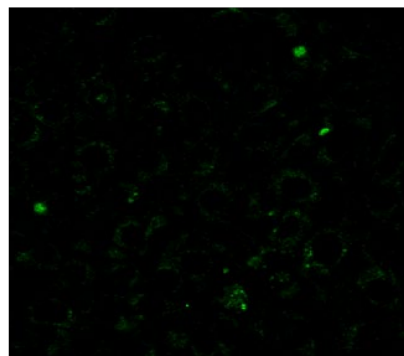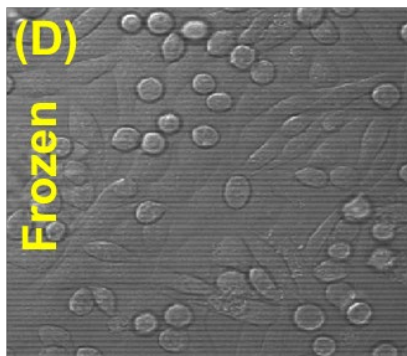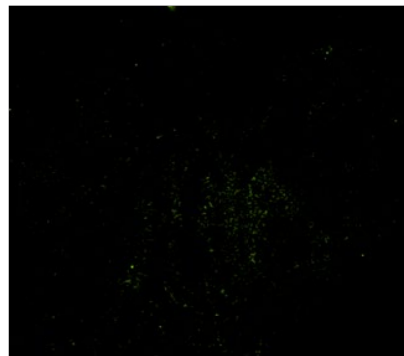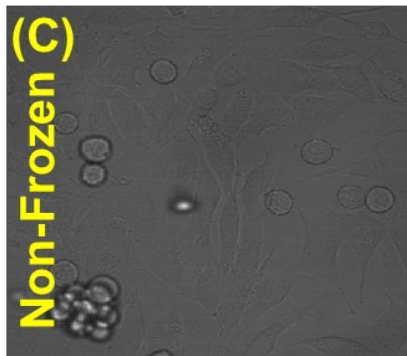
2

Polystyrene beads 50 nm

Bright field	Fluorescent
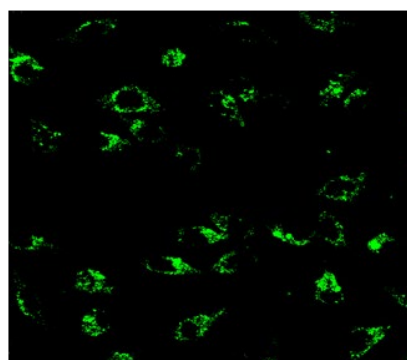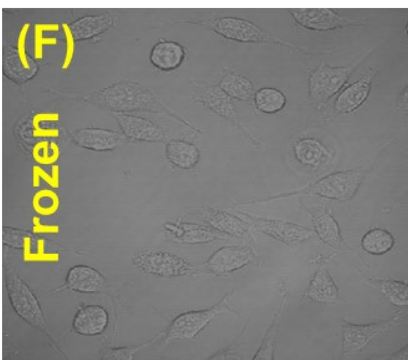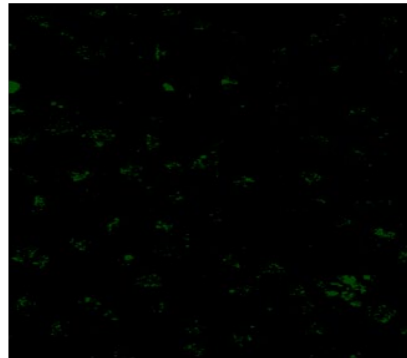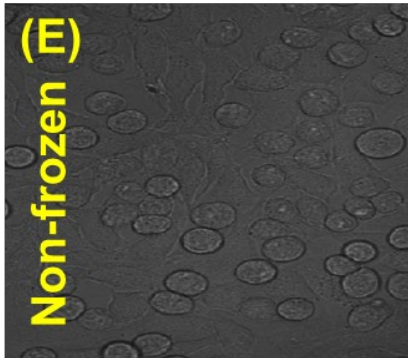
Polystyrene beads 100 nm
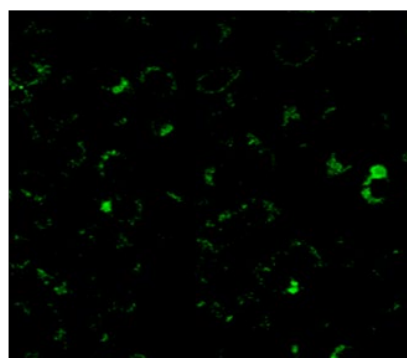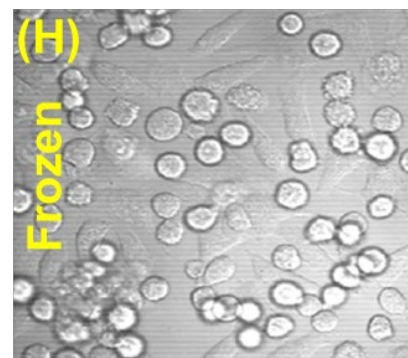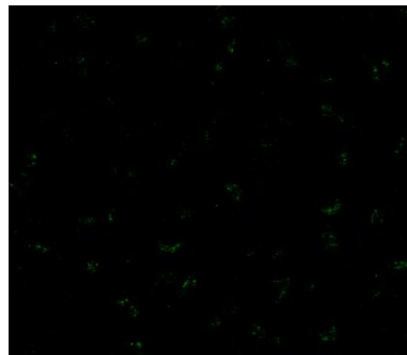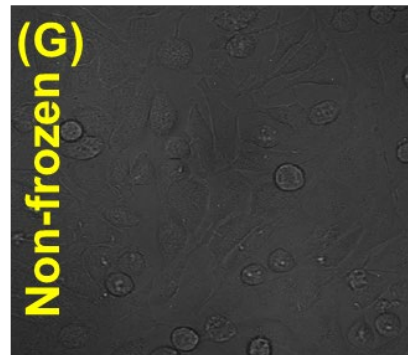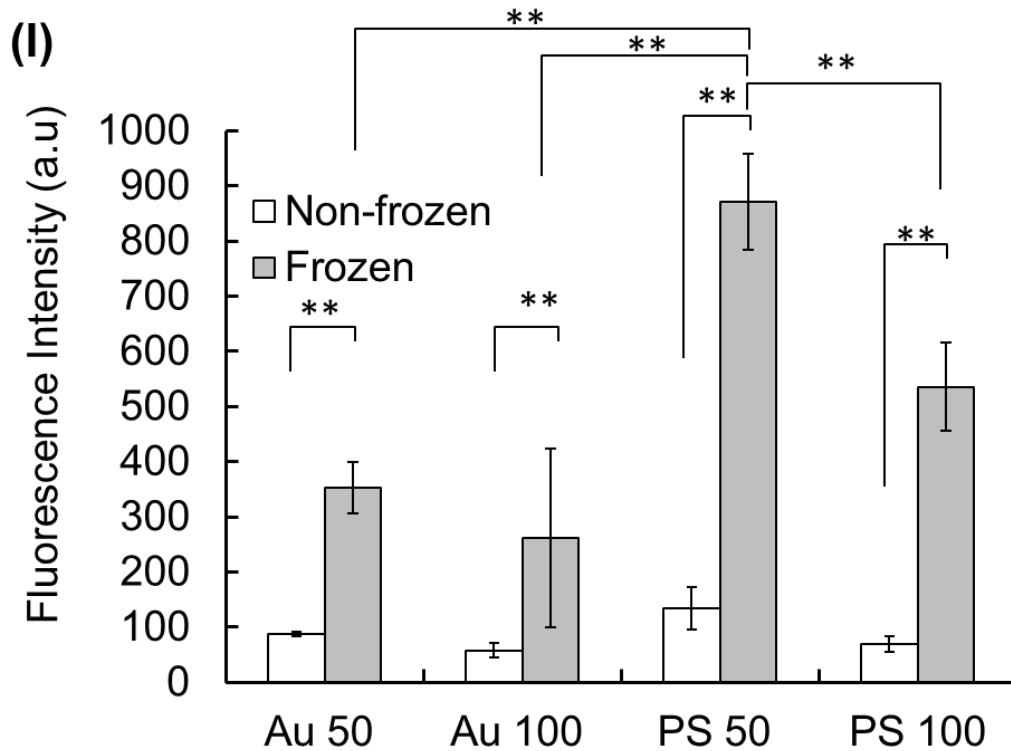
Figure 3 Internalisation of Au nanoparticles in L929 cells. (A, C) Without the freeze-concentration of Au nanoparticles of 50 and 100 nm (B, D) With the freeze concentration of Au nanoparticles at -80°C using 10% DMSO as a cryoprotectant. Internalisation of PS nanoparticles in L929 cells. (E, G) Without the freeze-concentration of PS nanoparticles of 50 and 100 nm. (F, H) With the freeze concentration of PS nanoparticles at -80°C using 10% DMSO as a cryoprotectant. Scale bar: 30 μm. (I) Mean intensities of scattering and fluorescence images of Au and PS nanoparticles were obtained by confocal microscopy. Results are expressed as means ± SD. **$p < 0.01$
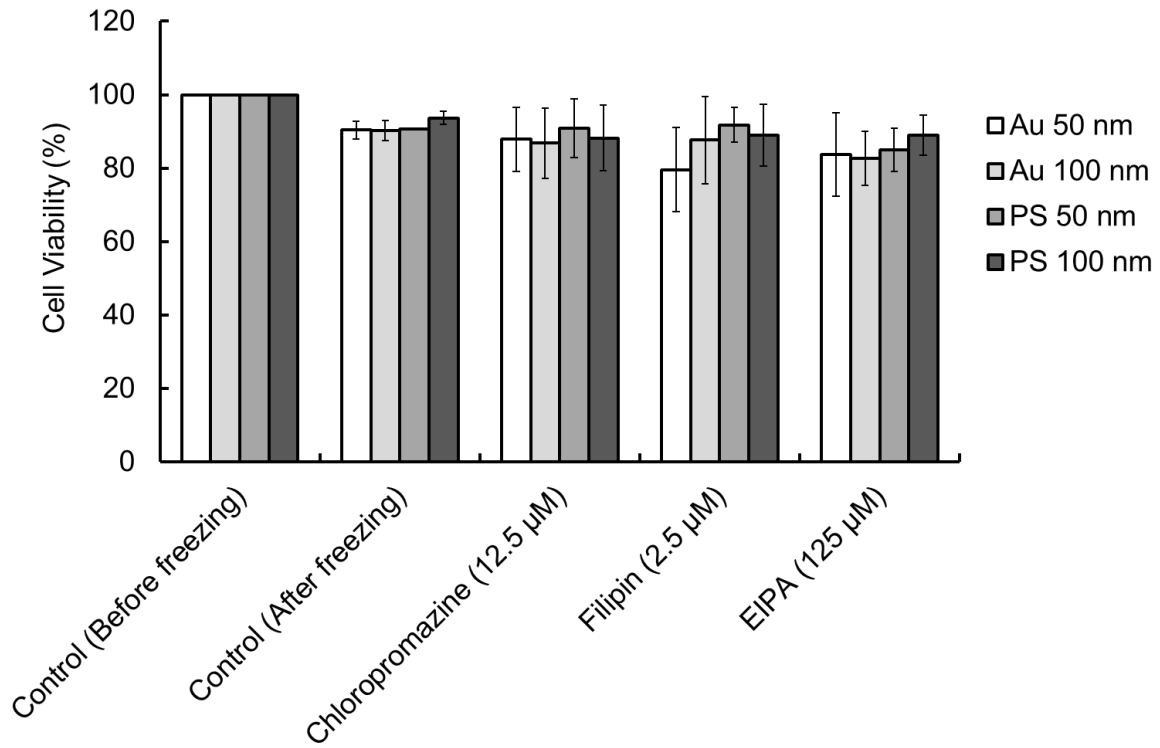
1

2 **Figure 4** Quantification of cell viability determined by trypan blue-exclusion assays after

3 the addition of endocytic inhibitors to Au and PS nanoparticles of 50 nm and 100 nm after
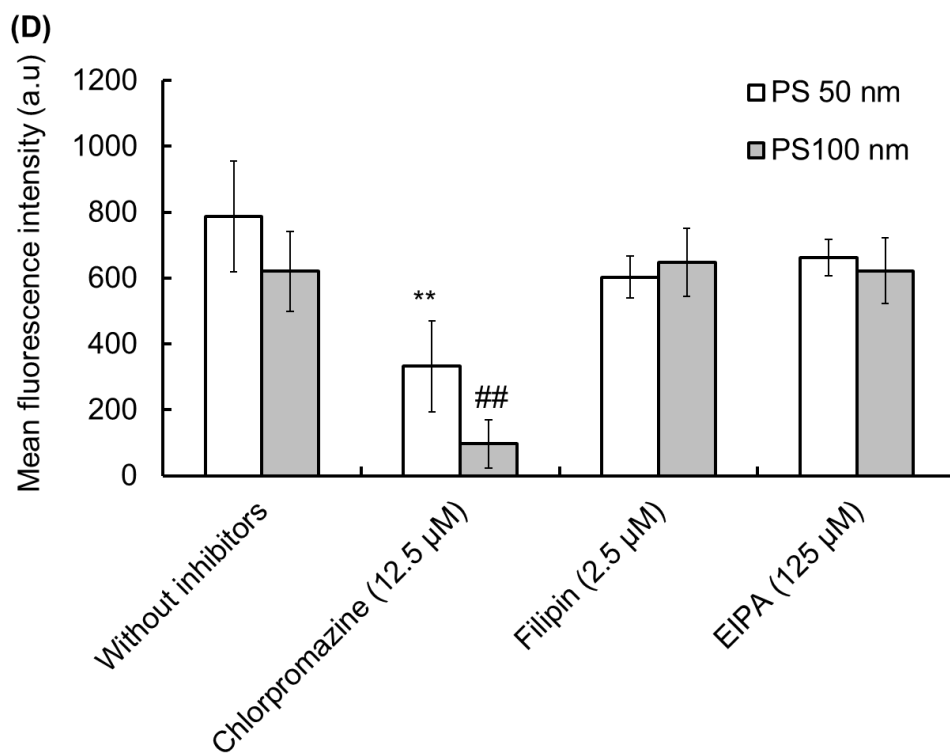
4 freezing. Results are expressed as means ± SD.

5

(A)

1

(B)

2

(C)

1

(D)

2
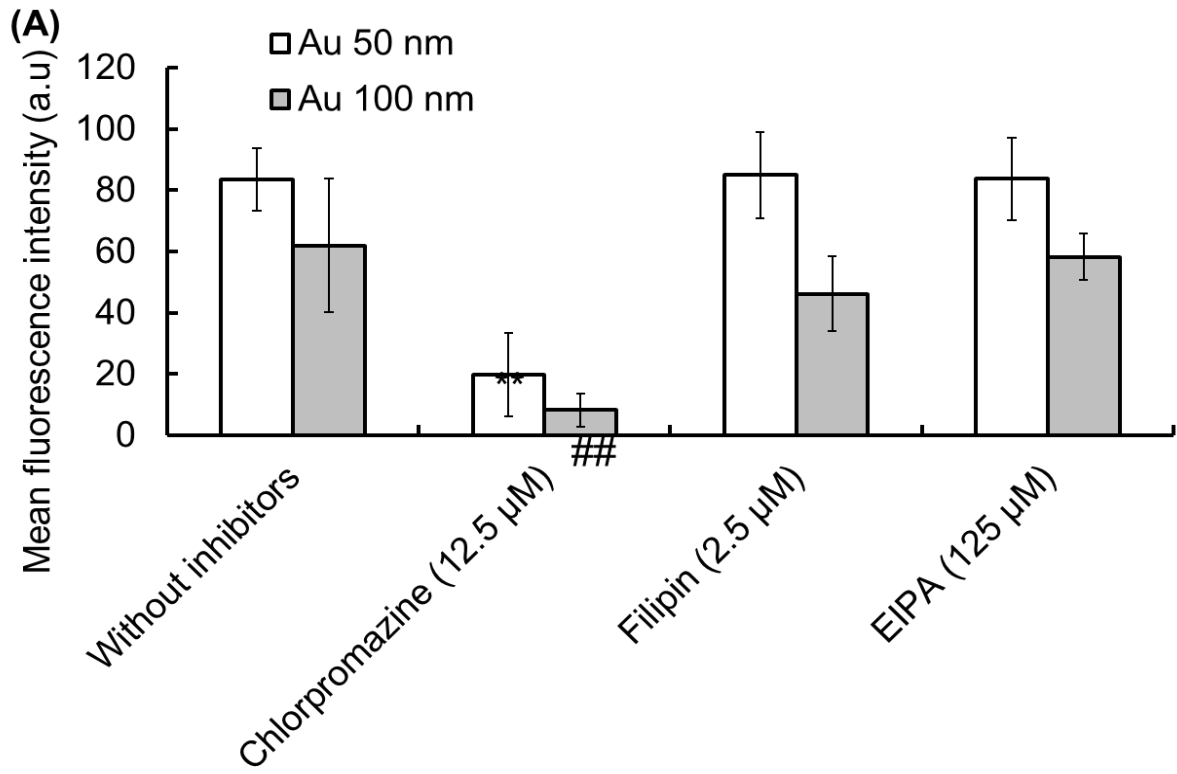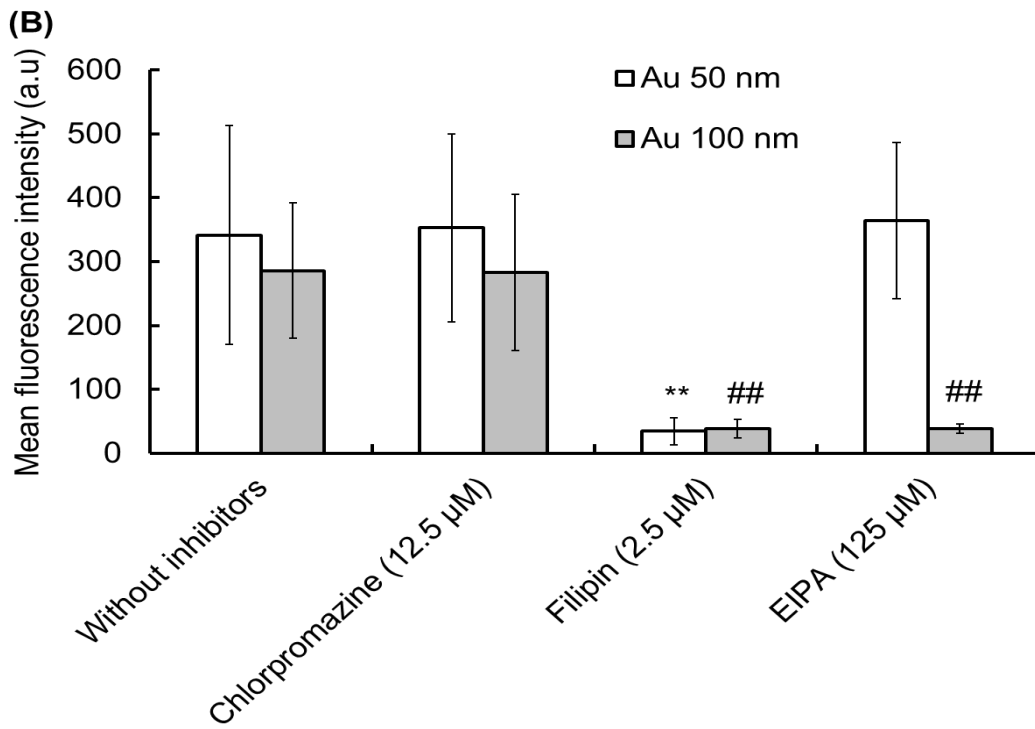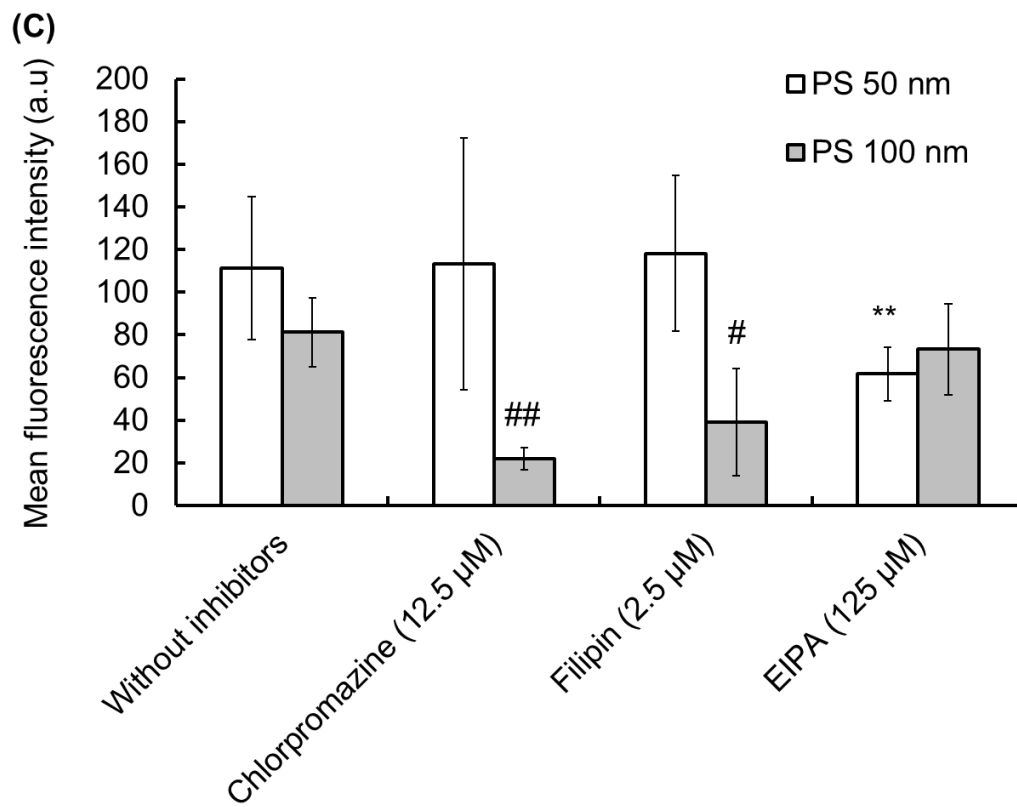
Figure 5 Quantitative analysis of the fluorescence/scattering intensity by confocal microscopy during endocytic uptake via clathrin-mediated endocytosis (ME), caveolae ME, and macropinocytosis ME, following treatment with various inhibitors. (A) Non-frozen Au 50 nm (B) Frozen Au 50 nm (C) Non-frozen PS 50 nm (D) Frozen PS 100 nm. Results are expressed as means ± SD. **$p < 0.01$, *$p < 0.05$ vs. without inhibitors for 50-nm nanoparticles and ##$p < 0.01$, #$p < 0.05$ vs. without inhibitors for 100-nm nanoparticles.

Electronic supplementary information (ESI) for

Comparative analysis of the cellular entry of polystyrene and gold nanoparticles using the freeze concentration method

Sana Ahmed, Koyo Okuma, and Kazuaki Matsumura*

School of Materials Science, Japan Advanced Institute of Science and Technology, Nomi, Ishikawa 923-1292, Japan
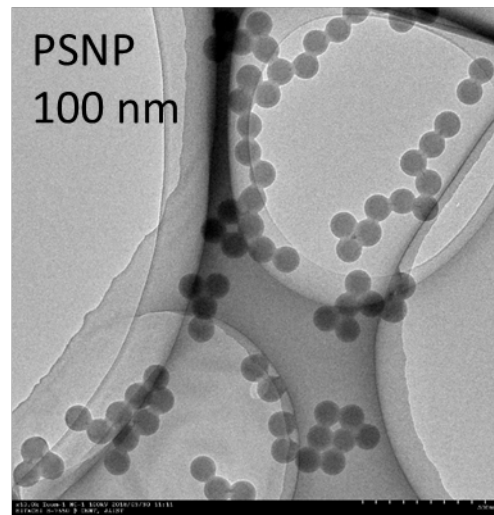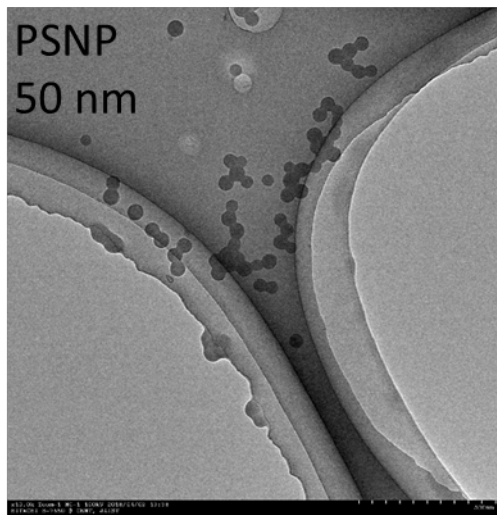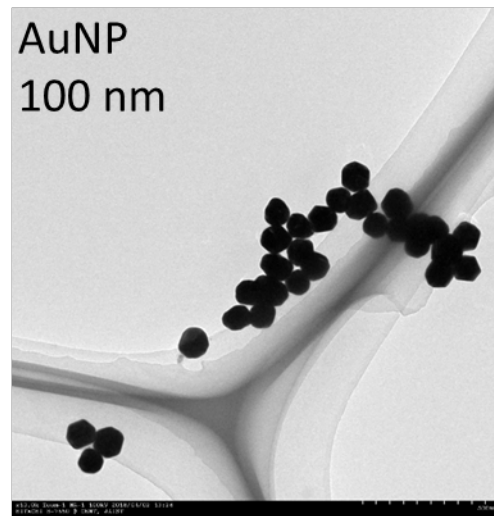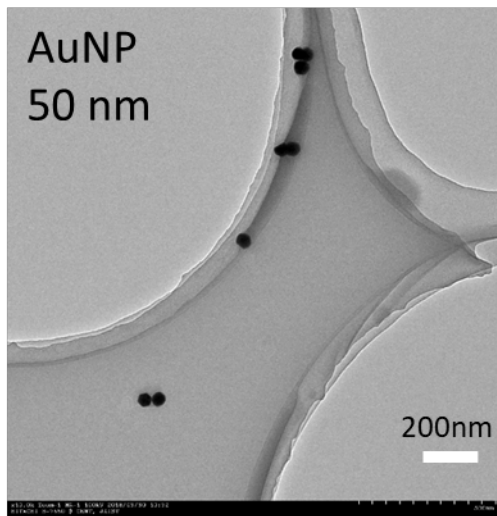
E mail: mkazuaki@jaist.ac.jp

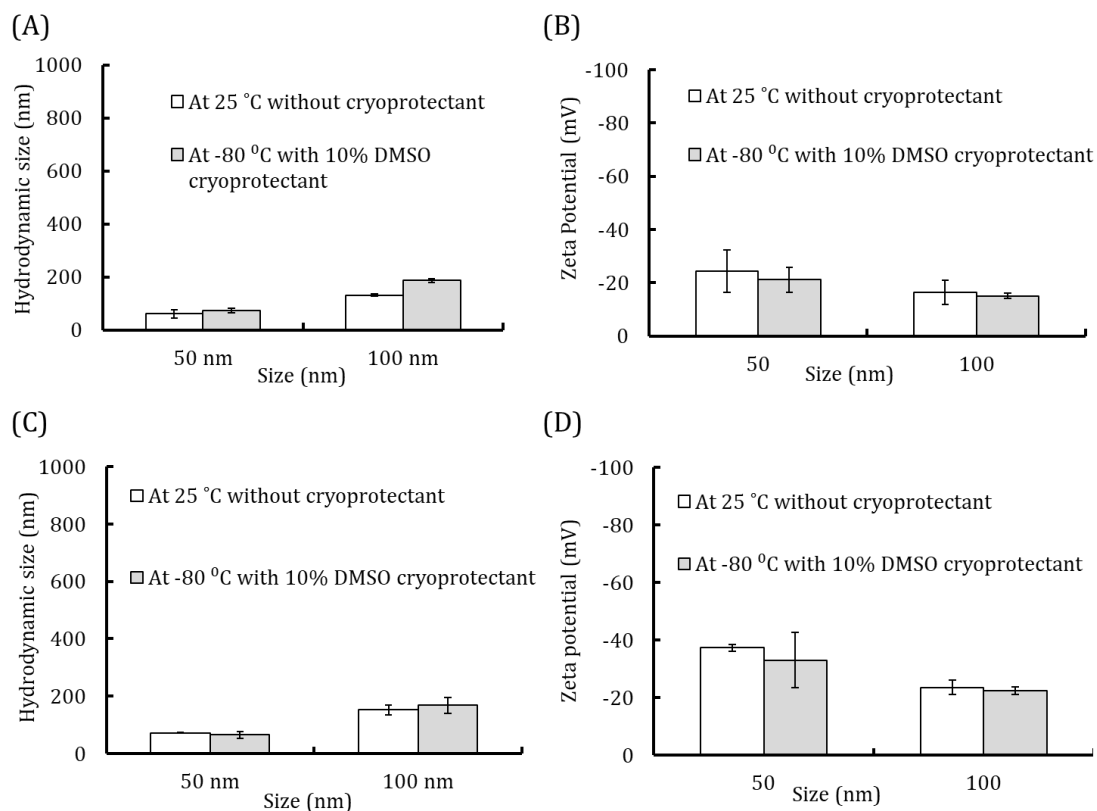**Figure S1** TEM images of Au and PS nanoparticles.

Figure S2 Hydrodynamic diameter and Zeta potential of nanoparticles at room temperature (25°C) with no cryoprotectant (White bars) and after freezing with 10% DMSO as a cryoprotectant at -80°C (Grey bars). Au nanoparticle (A) hydrodynamic diameter and (B) Zeta potential. PS nanoparticle (C) hydrodynamic diameter and (D) Zeta potential.
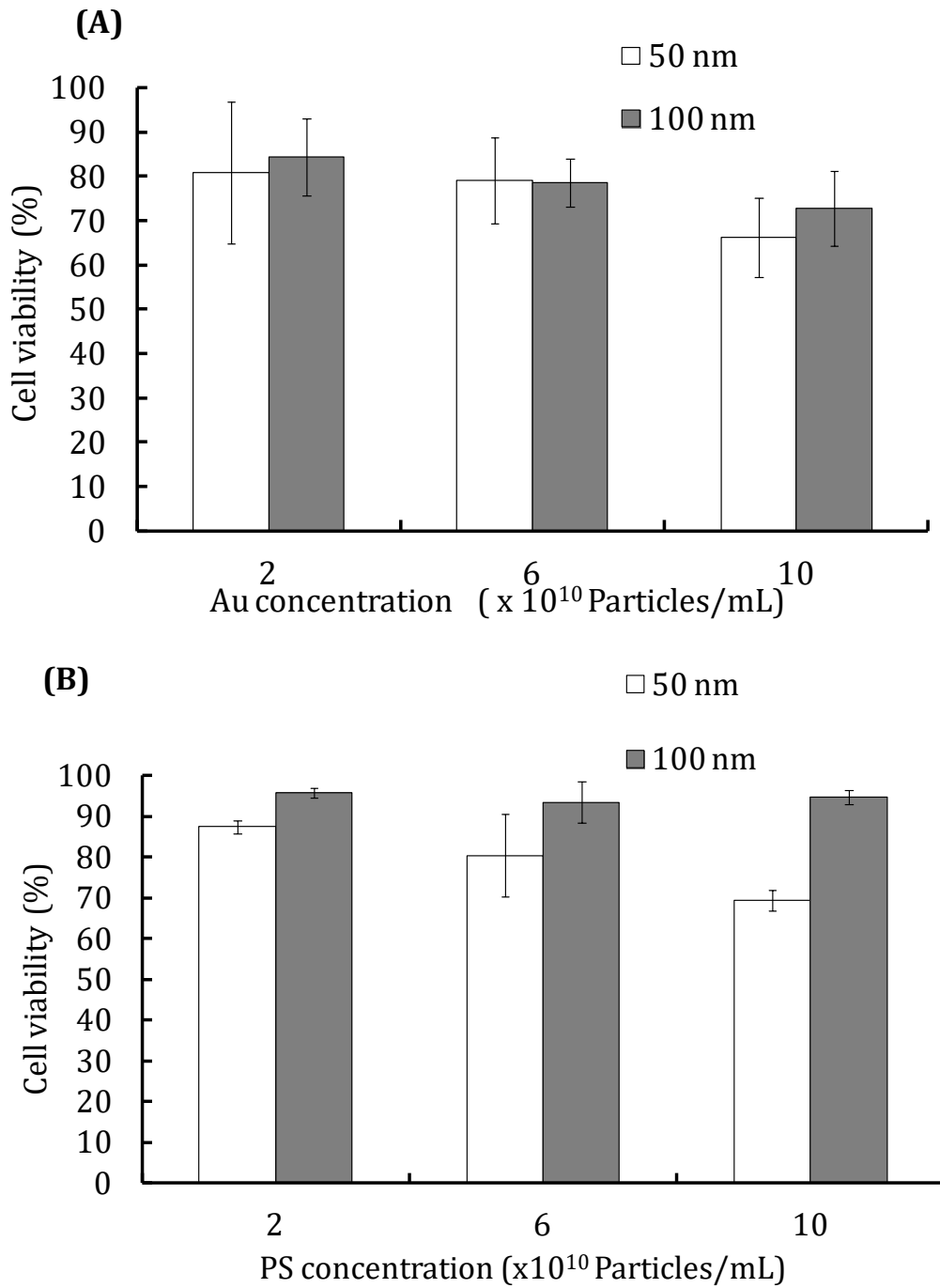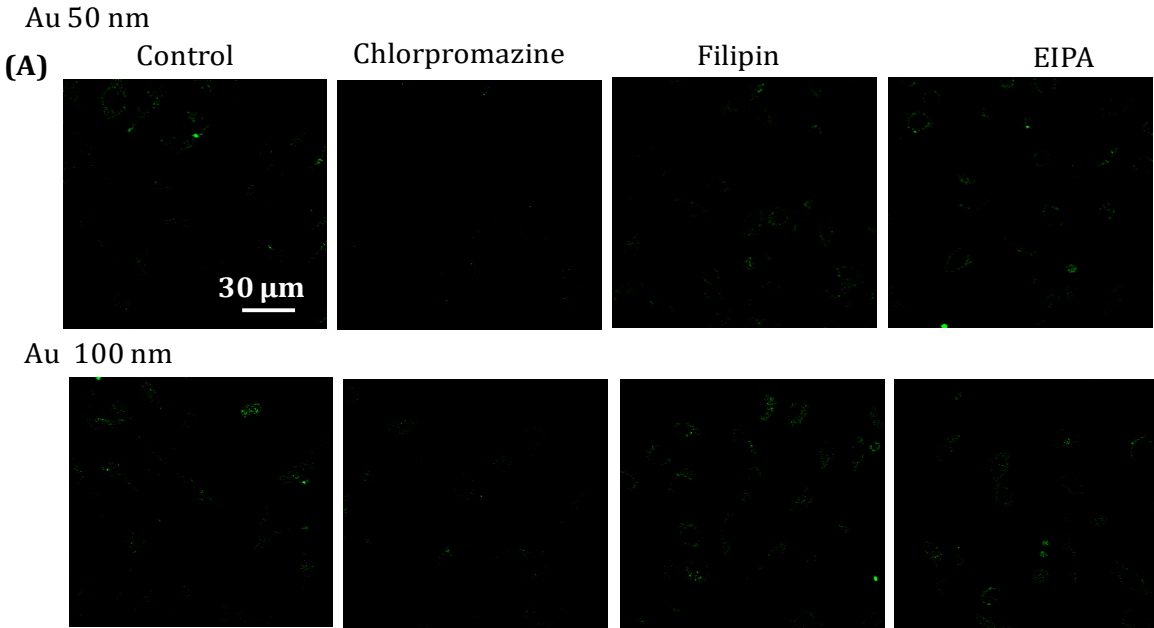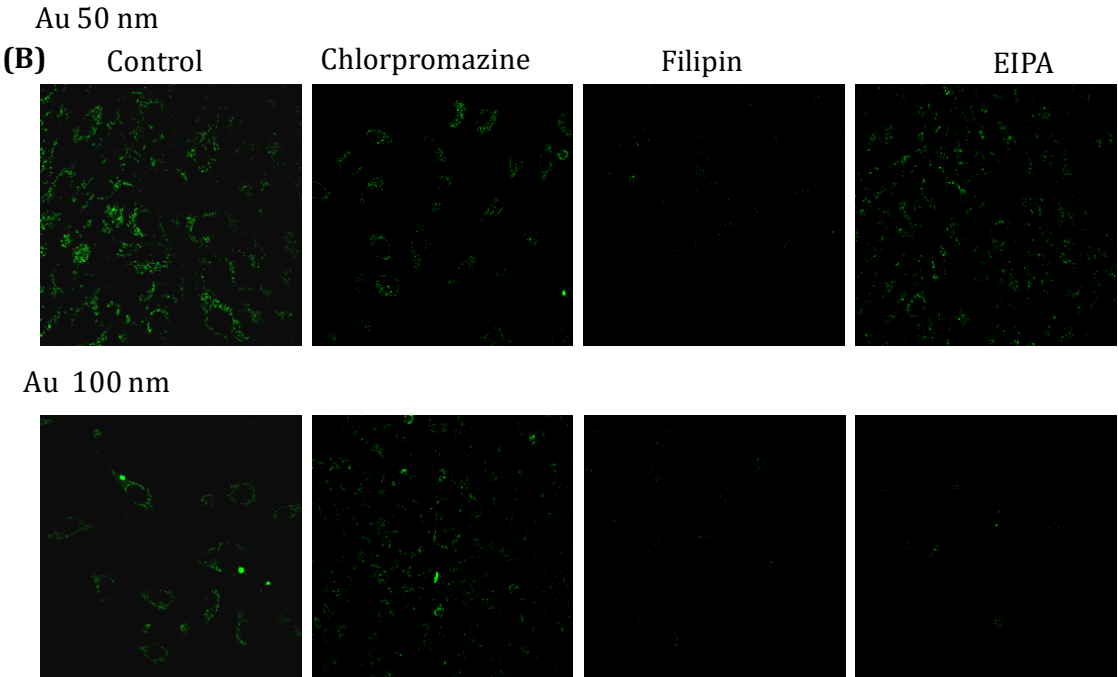
Figure S3 Cell viability using nanoparticles at various concentrations after freezing with 10% DMSO as a cryoprotectant, as determined by trypan blue exclusion assays, for (A) Au and (B) PS.

Non-Frozen

Au 50 nm

(A)

Control Chlorpromazine Filipin EIPA

30 μm

Au 100 nm

Frozen

Au 50 nm

(B)

Control Chlorpromazine Filipin EIPA

Au 100 nm

Non-Frozen

PS 50 nm

(C) Control   Chlorpromazine   Filipin   EIPA

30 μm

PS 100 nm

Frozen

PS 50 nm

(D) Control   Chlorpromazine   Filipin   EIPA
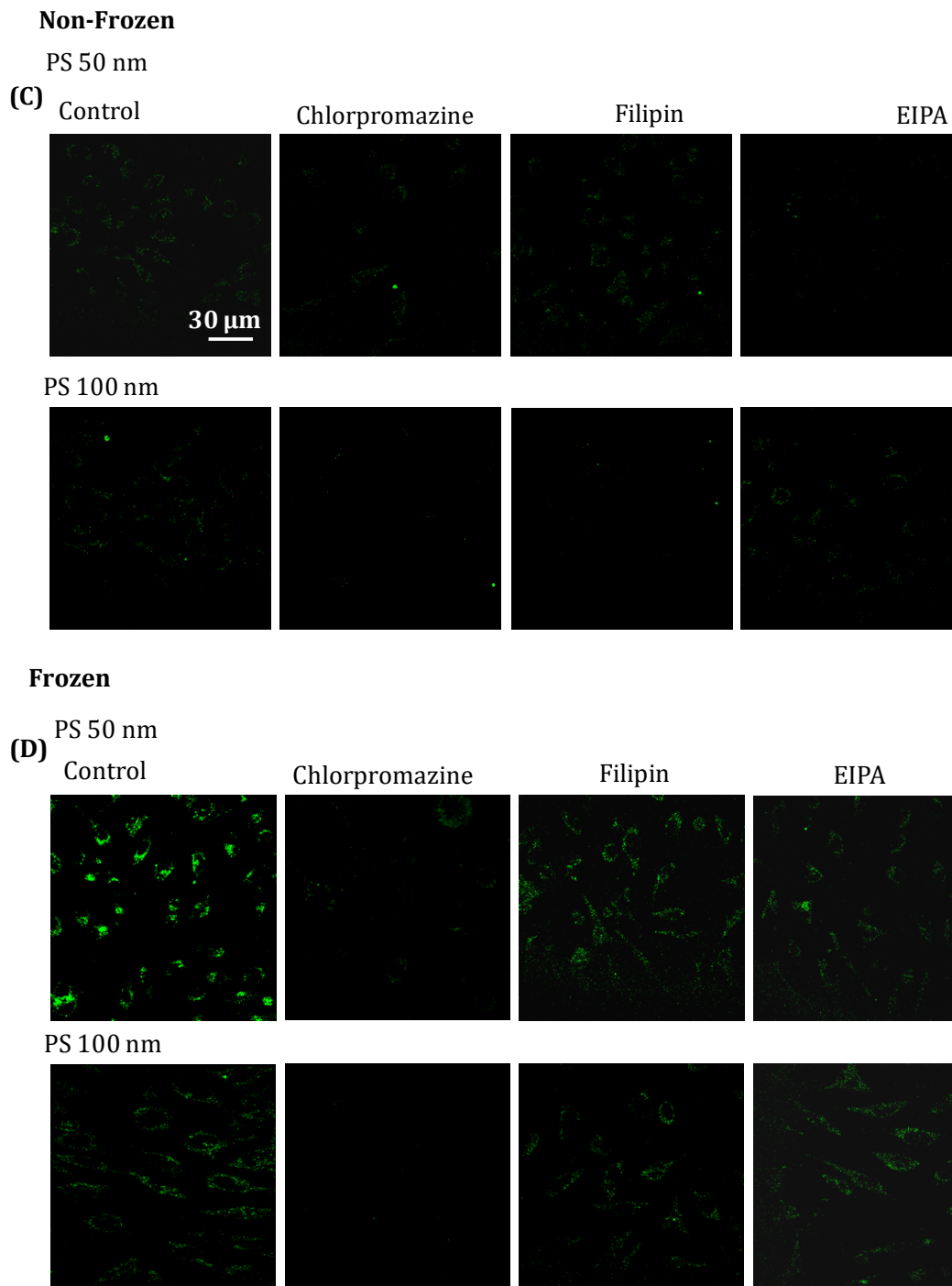

PS 100 nm

Figure S4 Confocal images of non-frozen and frozen endocytic uptake of 50- and 100-nm gold nanoparticles (A, B) or 50- and 100-nm polystyrene beads (C, D). For freezing, the samples were pre-incubated with inhibitors in the presence of 10% DMSO as a cryoprotectant. After thawing, the cells were seeded and incubated for at least 10 h. Scale bar: 30 μm.